

Strategic modification of ligands for remarkable piezochromic luminescence (PCL) based on a neutral Ir(III) phosphor[‡]

Dan Li,^a Guangfu Li,^a Jiaxin Xie,^a Dongxia Zhu,^{*a} Zhongmin Su^{*a} and Martin R. Bryce^{*b}

Received 00th January 20xx,
Accepted 00th January 20xx

DOI: 10.1039/x0xx00000x

www.rsc.org/

A new aggregation-induced emission (AIE)-active neutral Ir(III) complex has been rationally designed and synthesized by introducing carboxyl and F substituents into the ancillary and cyclometalating ligands, respectively, to construct different kinds of intermolecular interaction, leading to excellent piezochromic luminescence (PCL) properties. The emission colours are tunable by a grinding–fuming/heating process with good reversibility in the solid state. A combination of powder X-ray diffraction, differential scanning calorimetry, ¹H NMR, X-ray photoelectron and Fourier-transform infrared spectroscopy unambiguously confirm that the mechanism of PCL involves disruption of the intermolecular π – π interactions and hydrogen bonding. The combined AIE and PCL properties have enabled an efficient re-writable data recording device to be fabricated using the Ir(III) complex as the active material.

Introduction

Piezochromic luminescent (PCL) materials exhibit reversible switching of the emission in response to mechanical grinding and fuming or heating in the solid state.^{1–4} They have been extensively studied over the past decade as a class of ‘smart’ functional materials due to their promising potential as pressure sensors, optical devices and memory chips.^{5–11} Various small organic molecules,^{12, 13} polymers,^{14, 15} metal complexes,^{16, 17} co-crystals¹⁸, metal–organic frameworks¹⁹ and perovskites²⁰ with interesting PCL properties have been investigated. Especially, phosphorescent Ir(III) complexes have attracted extensive attention owing to their favourable photophysical properties, controllable excited-state characteristics and tunable emission colours.^{21–24}

Highly efficient emission in the solid state is beneficial for a PCL material, and the notorious aggregation caused quenching (ACQ) effect should be avoided.^{25, 26} Aggregation-induced emission (AIE) was established by Tang and co-workers in 2001 as an effective way to overcome ACQ.²⁷ In AIE systems, the molecules exhibit strong luminescence only upon aggregate formation which causes restricted intramolecular motion. Moreover, Chi and co-workers have proved that the luminescence enhancement resulting from AIE may provide a direction for the exploitation of high-efficiency

PCL materials.²⁸ Nevertheless, there remains considerable scope to develop design ideas for Ir(III) complexes with simultaneous AIE and PCL dual properties. The main reasons can be summarized as follows: i) a lack of a clear theoretical direction for the structure–property relationships of PCL materials; ii) choosing Ir(III) complexes with flexible long alkyl chain substituents to realize dual optical properties usually leads to poor stability and complicated synthesis routes.^{21, 29} Hence, it is still a challenge to develop an effective and facile design strategy to obtain Ir(III) complexes with excellent PCL features.

Controlling the molecular packing mode between stable crystalline states and metastable amorphous states without using chemical reactions is a common method for changing the emission characteristics of PCL materials.^{30–34} On the basis of Etter’s hydrogen-bond rule³⁵ and Kitaigorodskii’s close-packing principle,³⁶ hydrogen bonding and π – π interactions are two vital principles for designing tunable-state luminescent materials.³⁰ For instance, in this context Zhang and co-workers have shown that the interaction directed by hydrogen bonds can be exploited to control the molecular packing mode.³⁷ In previous reports, C=O and N–H substituents have been used to construct hydrogen bonds, and the strongly electron-accepting F substituents were also adopted to favour intermolecular interactions, such as π – π or C–H \cdots F interactions. These substituents have been utilized to realize PCL properties.^{24, 38–40} However, the carboxyl substituent is rarely reported for the construction of hydrogen bonds in PCL materials.^{41–43} In addition, in 2014 our group reported for the first time that introducing flexible Schiff base ligands into an iridium(III) complex is an effective method to achieve aggregation induced phosphorescent emission (AIPE) properties.⁴⁴

With these precedents in mind, we rationally designed and synthesized a neutral iridium(III) complex (abbreviated as complex **1**, Scheme 1), Ir(F₂ppy)₂(L) (L = carboxylated Schiff

^a Key Laboratory of Nanobiosensing and Nanobioanalysis at Universities of Jilin Province, Department of Chemistry, Northeast Normal University, 5268 Renmin Street, Changchun, Jilin Province 130024, P.R. China. E-mail: zhudx047@nenu.edu.cn; zmsu@nenu.edu.cn

^b Department of Chemistry, Durham University, Durham, DH1 3LE, UK. E-mail: m.r.bryce@durham.ac.uk

[†] Electronic Supplementary Information (ESI) available: Experimental details, ¹H NMR spectra and photophysical properties. See DOI: 10.1039/x0xx00000x

[‡] This article is in recognition of Martin R. Bryce’s 35 years as a research group leader at Durham University.

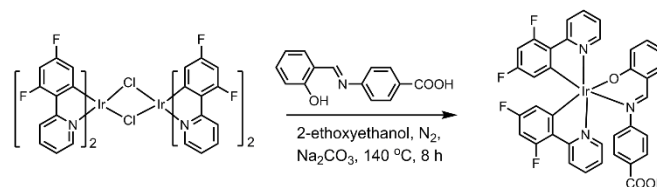
base ligand, $F_2ppy = 2-(2,4\text{-difluorophenyl})pyridine$). Herein, a flexible Schiff base ligand is selected to achieve the desired AIE properties. For the first time, the carboxyl substituents were successfully incorporated into ancillary ligands to form hydrogen bonds to realize PCL properties. At the same time, the strongly electron-accepting F substituents were attached to the cyclometalated ligands to favour intermolecular interaction such as $\pi\text{-}\pi$ and $C\text{-H}\cdots F$ interactions for effective PCL. The single-crystal X-ray structure analysis, 1H NMR spectra, powder X-ray diffraction (PXRD), differential scanning calorimetry (DSC), Fourier-transform infrared (FTIR) spectra, X-ray photoelectron spectroscopy (XPS) and detailed photophysical properties of complex **1** are presented. The results demonstrate that complex **1** exhibits significant AIE and PCL properties. We conclude that the carboxyl and F substituents play a key role in achieving PCL. More importantly, the emission colour of complex **1** can be reversibly switched upon fuming with organic solvent and this process can be cycled at least 5 times without any deterioration in the response. Additionally, an efficient proof-of-concept data recording device was fabricated using complex **1** as the active material.

Experimental section

Synthesis

The ancillary ligand **L** was easily synthesized as reported previously.⁴⁵ The cyclometalated chloride-bridged dimer $[Ir(F_2ppy)_2Cl]_2$ was obtained according to the literature by heating $IrCl_3\cdot 3H_2O$ and F_2ppy cyclometalated ligands in a mixture of water and 2-ethoxyethanol under nitrogen.⁴⁶ Complex **1** was obtained by the reaction of the ancillary ligand **L** with $[Ir(F_2ppy)_2Cl]_2$. Complex **1** was characterized by 1H NMR spectroscopy, mass spectrometry and elemental analysis.

Complex 1. A yellow suspension of the dichloro-bridged iridium complex $[Ir(F_2ppy)_2Cl]_2$ (0.182 g, 0.20 mmol), Schiff base bridging ligand (0.096 g, 0.40 mmol) and Na_2CO_3 (0.212 g, 2.0 mmol) in 2-ethoxyethanol was stirred at 140 °C for 8 h under a nitrogen atmosphere. The mixture was cooled to room temperature, the suspension was filtered, dried and purified by silica gel column chromatography with ethyl acetate/acetone (1:2 v/v) as eluent. The complex was obtained as a yellow solid in 63% yield (0.21 g). 1H NMR (500 MHz, $DMSO-d_6$, ppm): δ 12.80 (s, 1H), 8.98 (d, $J = 4$ Hz, 1H), 8.70 (d, $J = 4.5$ Hz, 1H), 8.31 (s, 1H), 8.25 (d, $J = 7$ Hz, 1H), 8.02-8.06 (m, 2H), 7.96 (d, $J = 7$ Hz, 1H), 7.53 (t, $J = 5$ Hz, 1H), 7.42-7.44 (m, 3H), 7.36 (d, $J = 5$ Hz, 1H), 7.23 (t, $J = 5$ Hz, 1H), 6.72 (t, $J = 7.5$ Hz, 1H), 6.50 (d, $J = 8.5$ Hz, 1H), 6.26-6.41 (m, 4H), 5.48 (d, $J = 7$ Hz, 1H), 5.44 (d, $J = 2.5$ Hz, 1H). MS: $m/z = 812.12$. Anal. calcd for $C_{36}H_{22}F_4IrN_3O_3$: C 53.20, H 2.73, N 5.17; found: C 53.16, H 2.75, N 5.13. Crystals for X-ray analysis were grown from a solution of **1** in ethyl acetate solvent.



Scheme 1 Synthetic route for complex **1**

Results and discussion

AIE behaviour

The photoluminescence quantum yield of complex **1** is 0.17 in the solid state (Table S2 in ESI). The AIE properties of complex **1** were investigated by emission and UV/vis absorption spectroscopy in different ratios of water- CH_3CN mixtures at room temperature. Complex **1** displayed almost no emission in CH_3CN solution, but the emission intensity significantly increased when the water fraction reached 80% (v/v). As shown in Fig. S4 (ESI \dagger), when the water fraction increased from 0% to 90%, the identical absorption peaks and the level-off tail appeared in the visible spectral region, due to the aggregates of complex **1** in the solvent mixture. The formation of nano-aggregates was further established by transmission electron microscopy (TEM) which indicated that the average sizes of spherical molecular aggregates increased obviously to about 120 nm (Figure S3b, ESI \dagger) when the water fraction was 90%.⁴⁷ Molecular aggregates are barely visible when complex **1** was in 0% water fraction (Figure S3a). The above results confirm that complex **1** is AIE active.

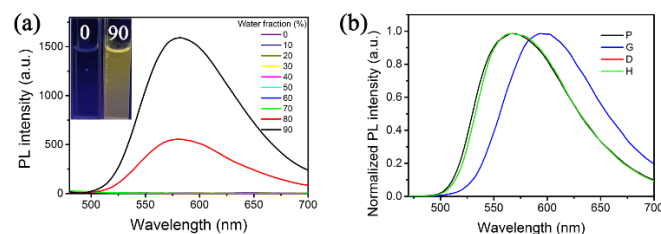


Fig. 1 (a) The emission spectra of complex **1** in water- CH_3CN mixtures with different water fractions (0–90% v/v) at room temperature. Inset: emission image of complex **1** in pure CH_3CN solution and a water- CH_3CN mixture (90% water fraction) under 365 nm UV illumination. (b) Normalized emission spectra of the samples as indicated.

Piezochromic behaviour

In order to verify the PCL properties of complex **1**, mechanical grinding experiments on the as-synthesized powders were performed. Under UV light irradiation, the pristine solid samples of complex **1** (hereafter referred to as **P**) exhibit yellow phosphorescence ($\lambda_{max} = 566$ nm) (Fig. 1b). Interestingly, when **P** was thoroughly ground by hand-pressure in an agate mortar for 20 s, a remarkable bathochromic shift (30 nm) was observed in the orange-emitting ground sample

(hereafter referred to as **G**), corresponding to $\lambda_{\max} = 596$ nm (Fig. 1b). These data confirm that **P** exhibits pressure-induced piezochromic behaviour. When exposed to dichloromethane (DCM) solvent (hereafter referred to as sample **D**), the orange-emitting samples reverted to the initial yellow emission colour within a few seconds. Notably, the emission colour could perfectly revert to **G** when **D** was further ground; this cycle was repeated at least 5 times (Fig. 2a). In addition to solvent-fuming, the emission colour of ground samples of PCL materials can also be reversibly switched to the original colour by other environmental stimuli, such as heating.²⁰ With this in mind, the changes of emission colour upon the grinding–heating processes of complex **1** were investigated. When **G** was heated at 180 °C, determined by the DSC data (see below), its emission colour changed from orange to yellow. By further grinding of the heated samples (hereafter referred to as **H**), the orange luminous powder was obtained again (Fig. 1b). From the above data, complex **1** exhibits multi-channel PCL behaviour and excellent reversibility for several grinding–fuming/heating cycles.

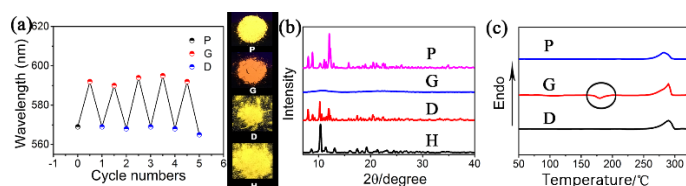


Fig. 2 (a) Repeated cycles of the grinding–fuming processes. Insets: emission images of **P**, **G**, **D**, and **H** under 365 nm UV illumination. (b) PXRD patterns and (c) DSC traces of the samples as indicated.

To investigate the origin and mechanism of the reversible piezochromic behaviour of complex **1**, the ¹H NMR spectra of **P** and **G** were obtained (Fig. S1 and S2, ESI†). The results showed that the chemical shift values and peak shapes of both samples were exactly the same, validating the fact that the phosphorescent colour changes in the grinding process are attributed to physical processes, such as changing the intermolecular interactions and/or the mode of the molecular packing.

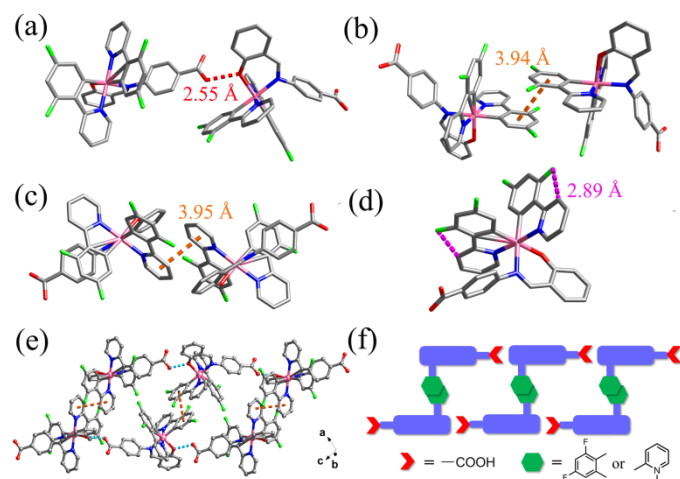


Fig. 3 (a) Intermolecular O-H...O hydrogen bonds; (b and c) π - π interactions; (d) intramolecular C-H...F interactions; (e) crystal structure; (f) schematic supramolecular structure of complex **1**.

The single crystal packing of complex **1** indicates the presence of multiple intermolecular interactions (Fig. 3). O-H...O hydrogen bonds with O...O distance of 2.55 Å connect molecules into a one-dimensional chain (Fig. 3a) and obvious intermolecular π - π interactions between the 2,4-difluorophenyl rings ($d = 3.94$ Å) (Fig. 3b) and neighbouring pyridine rings ($d = 3.95$ Å) (Fig. 3c) induce an ordered aggregation by connecting the one-dimensional chains. The introduction of carboxyl and F substituents successfully constructs a supramolecular two-dimensional network structure of complex **1**. Additionally, there are weak intramolecular C-H...F interactions ($d = 2.89$ Å) in the structure of complex **1** (Fig. 3d). Thus, this packing mode might be easily modified by mechanical stimuli resulting in the emission red-shift.

To gain more insight into the PCL mechanism of complex **1**, the PXRD data were obtained in various solid states. As depicted in Fig. 2b, the diffraction pattern of **P** displays numerous sharp and intense reflection peaks, confirming the existence of well-ordered aggregates. Conversely, very weak and broad diffraction signals are detected in **G**, which are different from those of **P**, revealing that **G** is amorphous. Therefore, it is established that the ordered structures of **P** are destroyed to a certain extent by grinding, leading to the amorphous states with red-shifted emission. Interestingly, after fuming with dichloromethane or heating **G**, the sharp and intense reflection peaks appeared again, confirming that recrystallization has been easily achieved by these processes. DSC experiments further confirm the formation of the amorphous powders upon grinding (Fig. 2c). For the DSC curves of **G**, an exothermic recrystallization peak appeared initially, and then an endothermic melting peak was detected, which is similar to the melting points of the corresponding crystalline state samples. It is known that the amorphous state will become less viscous and the molecules may obtain enough freedom of motion to spontaneously arrange themselves into crystalline forms as the temperature increases, indicating that the amorphized ground samples are in metastable states which can be restored to thermodynamically stable crystals through an exothermic recrystallization process.²⁹ Thus, based on the combined PXRD and DSC results, it appears that **G** investigated here comprises metastable amorphous states. If **G** is heated above the recrystallization temperatures, or is subjected to solvent-fuming, the amorphous states will revert to thermodynamically stable crystals through a recrystallization process.

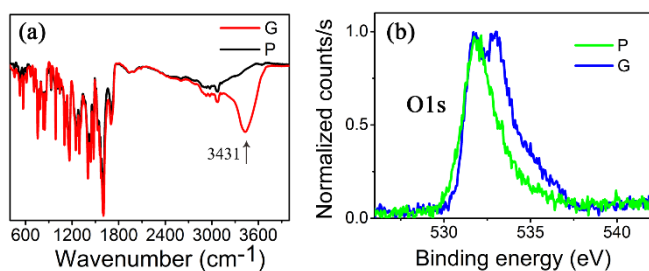


Fig. 4 FTIR spectra (a) and O 1s XPS spectra (b) of the samples as indicated.

The excited-state lifetimes (τ) for pristine (**P**) and ground (**G**) samples of complex **1** are significantly different with 2.31 and 2.15 μ s, respectively. Therefore, not only the emission colour but also the excited-state lifetimes of **1**, change as a result of the rearrangement of the molecular packing and intermolecular interactions.

The FTIR and the XPS data were obtained for **P** and **G** samples of complex **1**. As shown in Fig. 4a, unlike **P**, a new strong and broad peak at 3431 cm^{-1} appears in the FTIR spectrum of **G**, assigned to a free carboxyl group. The results demonstrate that the O-H \cdots O hydrogen bond was partially broken upon mechanical pressure. Fig. 4b shows the XPS spectrum of the O 1s regions for complex **1**. Additional O 1s signals at higher energy around 533.4 eV appeared upon grinding, which again indicates that the O-H \cdots O hydrogen bond was partially broken.⁴⁸ The FTIR and XPS data are, therefore, consistent. Moreover, the XPS spectra of F 1s, C 1s and N 1s regions all changed significantly, indicating that the π - π interaction between the neighbouring pyridine rings, the 2,4-difluorophenyl rings and intramolecular C-H \cdots F interactions were also changed in sample **G** (Fig. S5, ESI †). These results clearly prove that incorporation of the carboxyl and F substituents into complex **1** plays an important role in the PCL properties.



Fig. 5 Illustrations of the multi-channel photoluminescent colour changes of complex **1** (solution sample abbreviated as **S**).

By taking advantage of the combined AIE and reversible PCL properties of complex **1**, the different emission colours can be switched by heating, grinding, fuming and dissolution in solvent (Fig. 5).

Encouraged by the excellent piezochromic behaviour of complex **1**, a simple proof-of-concept re-writable phosphorescence data recording device has been fabricated (Fig. 6). The specific three-step procedure was as follows. (i) **G**

was evenly spread on a filter paper using an agate pestle to make a thin film exhibiting orange emission under UV excitation (λ 365 nm). (ii) Two yellow-emitting letters 'L' and 'Y' were written on the 'paper' using a 'pen' (made from a glass capillary) with DCM as the 'ink'. The letters show bright and distinctly different colour compared with the background. (iii) The letters 'L' and 'Y' were erased by grinding to recover the original orange background. This writing-erasing process can be repeated with excellent reversibility for at least five cycles. These results demonstrate that complex **1** is a candidate for practical applications as a security protection ink with simple optical authentication.

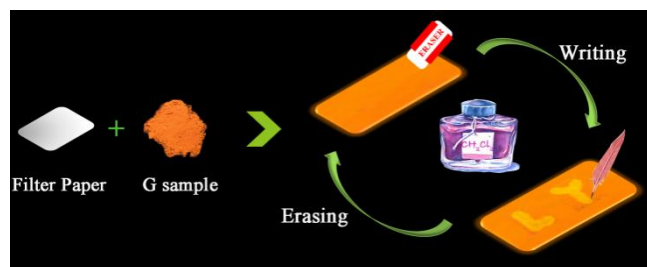


Fig. 6 A reversible data recording device of complex **1** based on its piezochromic and vapochromic phosphorescence.

Conclusions

In summary, a simple and rational strategy of ligand modification has led to a new 'smart' Schiff base Ir(III) complex which exhibits both reversible PCL and AIE behaviour. Intriguingly, the emission colour of **1** can be repeatedly switched between orange and yellow by grinding–fuming or grinding–heating processes. The grinding, fuming and heating processes took 20 seconds, 2 min and 5 min, respectively. Thereby a reversible and reproducible two-colour emission writing-erasing process was achieved. Based on the single crystal structure analysis, FTIR and XPS data, O-H \cdots O hydrogen bonds, intermolecular π - π interactions and weak intramolecular C-H \cdots F interactions are partially destroyed upon application of external stimuli, which result in the interconversion between crystalline and amorphous states, giving rise to the observed piezochromism. It is proposed that the carboxyl and F substituents play an important role in achieving PCL. We have now developed an effective and facile design strategy to obtain multi-functional Ir(III) complexes with excellent PCL features which provides a clear direction for exploiting the subtle structure-property relationships of PCL materials. The way is open to design new Ir(III) complexes, enrich the range of PCL materials and expand their applications in various fields.

Conflicts of interest

There are no conflicts to declare.

Acknowledgements

The work was funded by NSFC (No.51473028), the key scientific and technological project of Jilin province (20160307016GX, 20190701010GH), the Development and Reform Commission of Jilin province (20160058). The project was supported by Open Research Fund of State Key Laboratory of Polymer Physics and Chemistry, Changchun Institute of Applied Chemistry, Chinese Academy of Sciences. M. R. B. thanks EPSRC grant EL/L02621X/1 for funding.

Notes and references

- L. Bai, P. Bose, Q. Gao, Y. Li, R. Ganguly and Y. Zhao, *J. Am. Chem. Soc.*, 2017, **139**, 436-441.
- S. Biswas, D. Jana, G. S. Kumar, S. Maji, P. Kundu, U. K. Ghorai, R. P. Giri, B. Das, N. Chattopadhyay, B. K. Ghorai and S. Acharya, *ACS Appl. Mater. Interfaces*, 2018, **10**, 17409-17418.
- W. Z. Yuan, Y. Tan, Y. Gong, P. Lu, J. W. Y. Lam, X. Y. Shen, C. Feng, H. H. Y. Sung, Y. Lu, I. D. Williams, J. Z. Sun, Y. Zhang and B. Z. Tang, *Adv. Mater.*, 2013, **25**, 2837-2843.
- X. Zhang, Z. Chi, Y. Zhang, S. Liu and J. Xu, *J. Mater. Chem. C*, 2013, **1**, 3376-3390.
- Z. Chi, X. Zhang, B. Xu, X. Zhou, C. Ma, Y. Zhang, S. Liu and J. Xu, *Chem. Soc. Rev.*, 2012, **41**, 3878-3896.
- X. Hou, C. Ke, C. J. Bruns, P. R. McGonigal, R. B. Pettman and J. F. Stoddart, *Nat. Commun.*, 2015, **6**, 6884.
- M. Li, Q. Zhang, J.-R. Wang and X. Mei, *Chem. Commun.*, 2016, **52**, 11288-11291.
- Z. Song, R. Liu, Y. Li, H. Shi, J. Hu, X. Cai and H. Zhu, *J. Mater. Chem. C*, 2016, **4**, 2553-2559.
- H. Sun, S. Liu, W. Lin, K. Y. Zhang, W. Lv, X. Huang, F. Huo, H. Yang, G. Jenkins, Q. Zhao and W. Huang, *Nat. Commun.*, 2014, **5**, 3601.
- Z. Zhao, B. He and B. Z. Tang, *Chem. Sci.*, 2015, **6**, 5347-5365.
- X. Zhu, R. Liu, Y. Li, H. Huang, Q. Wang, D. Wang, X. Zhu, S. Liu and H. Zhu, *Chem. Commun.*, 2014, **50**, 12951-12954.
- (a) S. A. Sharber, K.-C. Shih, A. Mann, F. Frausto, T. E. Haas, M.-P. Nieh and S. W. Thomas, *Chem. Sci.*, 2018, **9**, 5415-5426; (b) Y. Zhang, K. Wang, G. Zhuang, Z. Xie, C. Zhang, F. Cao, G. Pan, H. Chen, B. Zou and Y. Ma, *Chem. Eur. J.*, 2015, **21**, 2474 - 2479; (c) L. Huang, Y. Qiu, C. Wu, Z. Ma, Z. Shen and X. Jia, *J. Mater. Chem. C*, 2018, **6**, 10250-10255; (d) X. Wu, J. Guo, Y. Cao, J. Zhao, W. Jia, Y. Chen and D. Jia, *Chem. Sci.*, 2018, **9**, 5270-5277; (e) C. Duan, Y. Zhou, G.-G. Shan, Y. Chen, W. Zhao, D. Yuan, L. Zeng, X. Huang and G. Niu, *J. Mater. Chem. C*, 2019, **7**, 3471-3478.
- (a) X. Wu, J. Guo, Y. Cao, J. Zhao, W. Jia, Y. Chen and D. Jia, *Chem. Sci.*, 2018, **9**, 5270-5277; (b) S. Jiang, J. Wang, Q. Qi, J. Qian, B. Xu, F. Li, Q. Zhou and W. Tian, *Chem. Commun.*, 2019, **55**, 3749-3752; (c) Q. Qi, J. Zhang, B. Xu, B. Li, Sean, X.-A. Zhang and W. Tian, *J. Phys. Chem. C*, 2013, **117**, 24997-25003.
- M. Andrzejewski, N. Casati and A. Katrusiak, *Dalton Trans.*, 2017, **46**, 14795-14803.
- Q. Sui, N.-N. Yang, T. Gong, P. Li, Y. Yuan, E.-Q. Gao and L. Wang, *J. Phys. Chem. Lett.*, 2017, **8**, 5450-5455.
- M. Jin, T. Seki and H. Ito, *Chem. Commun.*, 2016, **52**, 8083-8086.
- G.-G. Shan, H.-B. Li, H.-Z. Sun, D.-X. Zhu, H.-T. Cao and Z.-M. Su, *J. Mater. Chem. C*, 2013, **1**, 1440-1449.
- Y. Liu, Q. Zeng, B. Zou, Y. Liu, B. Xu and W. Tian, *Angew. Chem. Int. Ed.*, 2018, **57**, 15670-15674.
- (a) A. K. Chaudhari and J.-C. Tan, *Nanoscale*, 2018, **10**, 3953-3960; (b) H. Li, X. Zhang, Z. Chi, B. Xu, W. Zhou, S. Liu, Y. Zhang and J. Xu, *Org. Lett.*, 2011, **13**, 556-559.
- (a) R. Zhang, W. Cai, T. Bi, N. Zarifi, T. Terpstra, C. Zhang, Z. V. Verdeny, E. Zurek and S. Deemyad, *J. Phys. Chem. Lett.*, 2017, **8**, 3457-3465; (b) Y. Wang, X. Lu, W. Yang, T. Wen, L. Yang, X. Ren, L. Wang, Z. Lin and Y. Zhao, *J. Am. Chem. Soc.*, 2015, **137**, 11144-11149.
- Y. Han, H.-T. Cao, H.-Z. Sun, G.-G. Shan, Y. Wu, Z.-M. Su and Y. Liao, *J. Mater. Chem. C*, 2015, **3**, 2341-2349.
- Y. Jiang, G. Li, W. Che, Y. Liu, B. Xu, G. Shan, D. Zhu, Z. Su and M. R. Bryce, *Chem. Commun.*, 2017, **53**, 3022-3025.
- Y. Jiang, G. Li, D. Zhu, Z. Su and M. R. Bryce, *J. Mater. Chem. C*, 2017, **5**, 12189-12193.
- Y. Wang, T. Yang, X. Liu, G. Li, W. Che, D. Zhu and Z. Su, *J. Mater. Chem. C*, 2018, **6**, 12217-12223.
- Y.-B. Gong, P. Zhang, Y.-r. Gu, J.-Q. Wang, M.-M. Han, C. Chen, X.-J. Zhan, Z.-L. Xie, B. Zou, Q. Peng, Z.-G. Chi and Z. Li, *Adv. Opt. Mater.*, 2018, **6**, 1800198.
- Y. Qi, N. Ding, Z. Wang, L. Xu and Y. Fang, *ACS Appl. Mater. Interfaces*, 2019, **11**, 8676-8684.
- J. Luo, Z. Xie, J. W. Lam, L. Cheng, H. Chen, C. Qiu, H. S. Kwok, X. Zhan, Y. Liu, D. Zhu and B. Z. Tang, *Chem. Commun.*, 2001, 1740-1741.
- B. Xu, J. He, Y. Mu, Q. Zhu, S. Wu, Y. Wang, Y. Zhang, C. Jin, C. Lo, Z. Chi, A. Lien, S. Liu and J. Xu, *Chem. Sci.*, 2015, **6**, 3236-3241.
- Y. Han, H.-T. Cao, H.-Z. Sun, Y. Wu, G.-G. Shan, Z.-M. Su, X.-G. Hou and Y. Liao, *J. Mater. Chem. C*, 2014, **2**, 7648-7655.
- Y. Dong, B. Xu, J. Zhang, X. Tan, L. Wang, J. Chen, H. Lv, S. Wen, B. Li, L. Ye, B. Zou and W. Tian, *Angew. Chem. Int. Ed.*, 2012, **51**, 10782-10785.
- Y. Dong, J. Zhang, X. Tan, L. Wang, J. Chen, B. Li, L. Ye, B. Xu, B. Zou and W. Tian, *J. Mater. Chem. C*, 2013, **1**, 7554-7559.
- Q. Qi, J. Qian, X. Tan, J. Zhang, L. Wang, B. Xu, B. Zou and W. Tian, *Adv. Funct. Mater.*, 2015, **25**, 4005-4010.
- Y. Sagara and T. Kato, *Angew. Chem. Int. Ed.*, 2008, **47**, 5175-5178.
- P. Xue, J. Ding, P. Wang and R. Lu, *J. Mater. Chem. C*, 2016, **4**, 6688-6706.
- M. C. Etter, *Acc. Chem. Res.*, 1990, **23**, 120-126.
- A. I. Kitaigorodskii, *Organic Chemical Crystallography*, Consultants Bureau, New York, 1961.
- R. Huang, C. Wang, Y. Wang and H. Zhang, *Adv. Mater.*, 2018, **30**, 1800814.
- E. Nagata, S. Takeuchi, T. Nakanishi, Y. Hasegawa, Y. Mawatari and H. Nakano, *Chemphyschem*, 2015, **16**, 3038-3043.
- P. Sudhakar, K. K. Neena and P. Thilagar, *J. Mater. Chem. C*, 2017, **5**, 6537-6546.
- H. Yu, W. Ren, H. Lu, Y. Liang and Q. Wang, *Chem. Commun.*, 2016, **52**, 7387-7389.
- L. D'Ascenzo and P. Auffinger, *Acta. Crystallogr., Sect. B: Struct. Sci.*, 2015, **71**, 164-175.
- S. Lis, Z. Glatty, G. Meinrath and M. Kubicki, *J. Chem. Crystallogr.*, 2010, **40**, 646-649.
- B. Lu, Y. Zhang, X. Yang, K. Wang, B. Zou and D. Yan, *J. Mater. Chem. C*, 2018, **6**, 9660-9666.

44. G. Li, X. Ren, G. Shan, W. Che, D. Zhu, L. Yan, Z. Su and M. R. Bryce, *Chem. Commun.*, 2015, **51**, 13036-13039.
45. S. K. Shrivastava, P. Srivastava, T. V. R. Upendra, P. N. Tripathi and S. K. Sinha, *Bioorg. Med. Chem.*, 2017, **25**, 1471-1480.
46. K. A. King, P. J. Spellane and R. J. Watts, *J. Am. Chem. Soc.*, 1985, **107**, 1431-1432.
47. G.-G. Shan, H.-B. Li, J.-S. Qin, D.-X. Zhu, Y. Liao and Z.-M. Su, *Dalton Trans.*, 2012, **41**, 9590-9593.
48. R. Flamia, G. Lanza, A. M. Salvi, J. E. Castle and A. M. Tamburro, *Biomacromolecules*, 2005, **6**, 1299-1309.

Electronic Supplementary Information (ESI)

Strategic modification of ligands for remarkable piezochromic luminescence (PCL) based on a neutral Ir(III) phosphor

Dan Li,^a Guangfu Li,^a Jiaxin Xie,^a Dongxia Zhu,^{*a} Zhongmin Su^{*a} and
Martin R. Bryce^{*b}

^a *Key Laboratory of Nanobiosensing and Nanobioanalysis at Universities of Jilin Province, Department of Chemistry, Northeast Normal University, 5268 Renmin Street, Changchun, Jilin Province 130024, P.R. China.*

E-mail: zmsu@nenu.edu.cn; zhudx047@nenu.edu.cn

^b *Department of Chemistry, Durham University, Durham, DH1 3LE, UK.*

E-mail: m.r.bryce@durham.ac.uk

Table of Contents

1. Experimental - general information	S3
2. ¹H NMR spectrum of complex 1 at room temperature	S4
3. X-ray crystallographic data	S4
4. Photophysical, TEM and XPS properties	S5

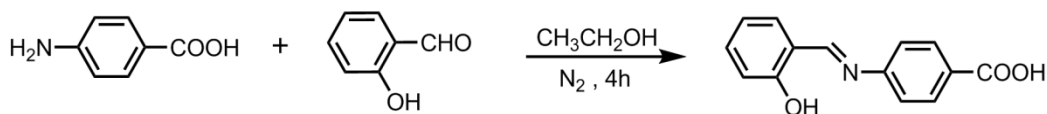
1. Experimental - general information

Materials obtained from commercial suppliers were used without further purification unless otherwise stated. All glassware, syringes, magnetic stirring bars, and needles were thoroughly dried in a convection oven. Reactions were monitored using thin layer chromatography (TLC). Commercial TLC plates were used and the spots were visualized under UV light at 254 and 365 nm. ^1H NMR spectra were recorded at 25 °C on a Varian 500 MHz spectrometer and were referenced internally to the residual proton resonance in $\text{DMSO-}d_6$ (δ 2.5 ppm). Mass spectra were obtained on matrix-assisted laser desorption-ionization time-of-flight (MALDI-TOF) mass spectrometry instrument. Elemental analyses were measured on a Flash EA1112 analyzer. Transmission electron microscopy (TEM) and electron diffraction analyses of the samples were obtained using a TECNAI F20 microscope. The samples were prepared by placing microdrops of the solution on a holey carbon copper grid. UV-vis absorption spectra were recorded on a Shimadzu UV-3100 spectrophotometer. The emission spectra were recorded by an F-7000 FL spectrophotometer. The excited-state lifetime and photoluminescence quantum yields (PLQYs) were measured using a transient spectrofluorimeter (Edinburgh FLS920). X-ray photoelectron spectroscopy (XPS) analyses were performed on a Quantum 2000 spectrometer. Powder X-ray diffraction (PXRD) patterns were obtained with a Rigaku Dmax 2000 instrument. Differential scanning calorimetry (DSC) curves were collected on a NETZSCH thermal analysis DSC200 F3 instrument under argon with a heating rate 10 °C min⁻¹. FTIR spectra were recorded on a Magna 560 FTIR spectrometer with KBr disks. The X-ray crystal data was obtained on a Bruker Smart Apex II CCD diffractometer with graphite-monochromated Cu K α radiation ($\lambda = 1.54178$).

Synthesis of Schiff base ligand

4-Aminobenzoic acid (0.274 g, 2.0 mmol) and salicylaldehyde (0.200 g, 1.63 mmol) were refluxed in ethanol (20 mL) at 78 °C for 5 h under a nitrogen atmosphere. The suspension was filtered, dried and purified by silica gel column chromatography with

ethyl acetate/acetone (2:1 v/v) as eluent. The Schiff base was obtained as a yellow solid in 82% yield (0.320 g).



Scheme S1 Synthetic route for Schiff base ligand

2. ^1H NMR Spectrum of complex **1** at room temperature

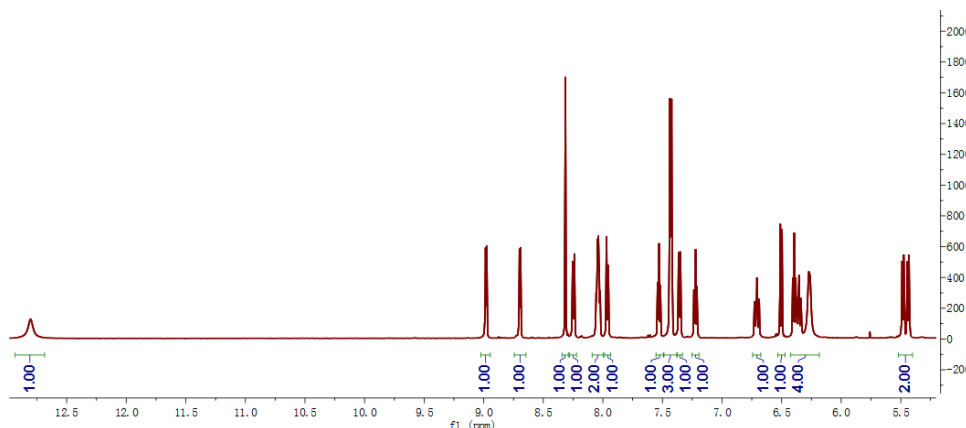


Fig. S1 ^1H NMR spectrum of complex **1** in $\text{DMSO-}d_6$ at room temperature.

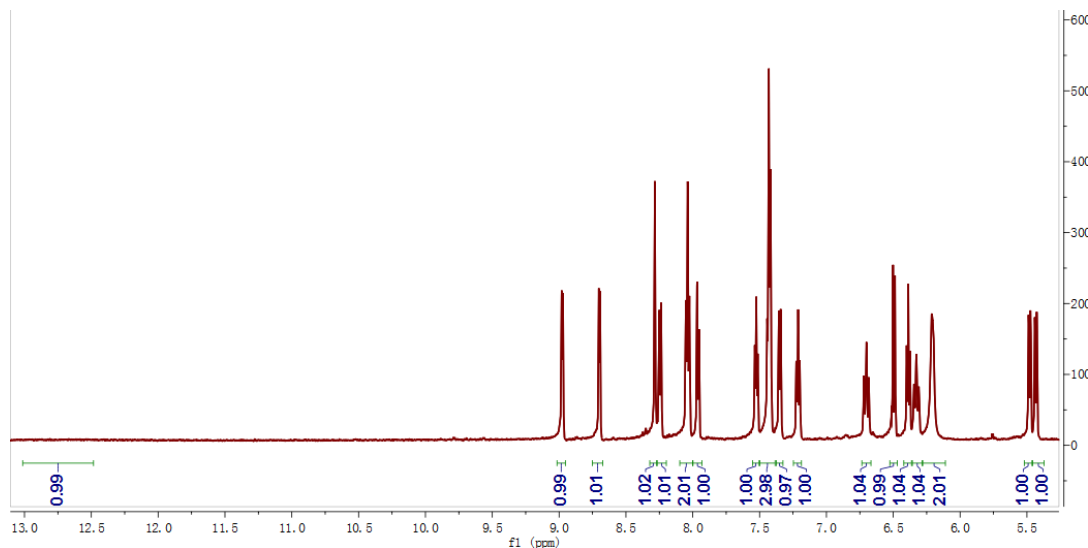


Fig. S2 ^1H NMR spectrum of complex **1** after grinding in $\text{DMSO-}d_6$ at room temperature.

3. X-ray crystallographic data

Diffraction data were collected on a Bruker SMART Apex CCD diffractometer using $\text{Cu K}\alpha$ ($\lambda = 1.54178$). Cell refinement and data reduction were made by the SAINT program. The structures were determined using the SHELXTL/PC program. The crystallographic data have been deposited with the Cambridge Crystallographic Data Centre with CCDC deposition number 1922460. These data can be obtained free of

charge from The Cambridge Crystallographic Data Centre via www.ccdc.cam.ac.uk/data_request/cif.

Table S1 Crystal data and structure refinement for complex **1**.

1	
Empirical formula	C ₃₆ H ₂₂ F ₄ IrN ₃ O ₃
Formula weight	813.12
Temperature (K)	298
Crystal system	monoclinic
space group	P2 ₁ /n
a /Å	17.686(3)
b /Å	10.9614(16)
c /Å	19.865(3)
α /°	90
β /°	106.682(8)
γ /°	90
V/Å ³	3688.9(10)
Z	4
ρ _{calc} (g/cm ³)	1.622
μ/mm ⁻¹	7.595
R _{int}	0.0535
Goodness-of-fit on F ²	1.095
R ₁ ^a , wR ₂ ^b [I>2σ(I)]	0.0268,0.0602
R ₁ , wR ₂ (all data)	0.0352,0.0641

^a R₁ = Σ||F_o| - |F_c||/Σ|F_o|. ^b wR₂ = { Σ[w(F_o² - F_c²)²] / Σ[w(F_o²)²] }^{1/2}

4. Photophysical, TEM and XPS properties

Table S2 Photophysical characteristics of complex **1**

Absorption and emission at room temperature				$k_r \times 10^6 \text{ s}^{-1}$	$k_{nr} \times 10^6 \text{ s}^{-1}$
λ_{abs}^a (nm)	λ_{em}^b (nm)	Φ_{em}^b	τ^b [μs]		
285, 390	566	0.17	2.31	0.07	0.36

^a Measured in CH₃CN (1.0×10⁻⁵ M) solution. ^b Measured in solid state (λ_{ex} = 400 nm;

error for Φ_{em} ± 5 %).

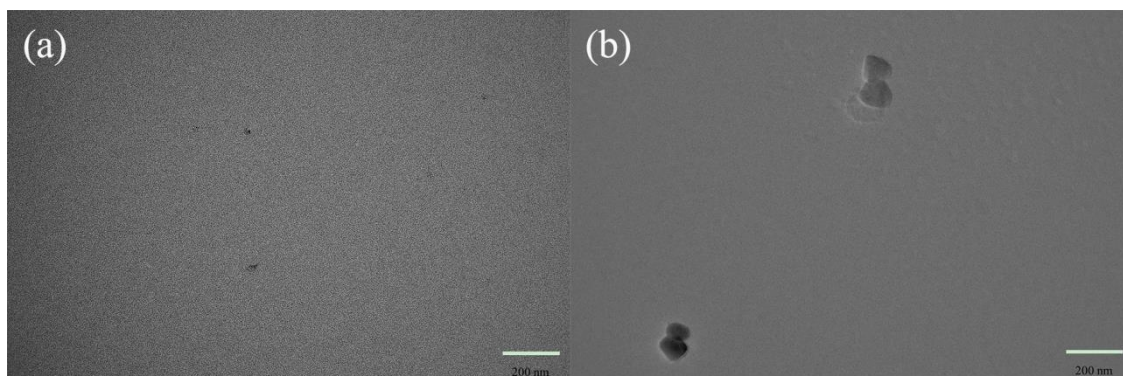


Fig. S3 TEM image of nanoaggregates of complex **1** formed in water-CH₃CN mixtures with 0% (a) and 90% (b) water fraction.

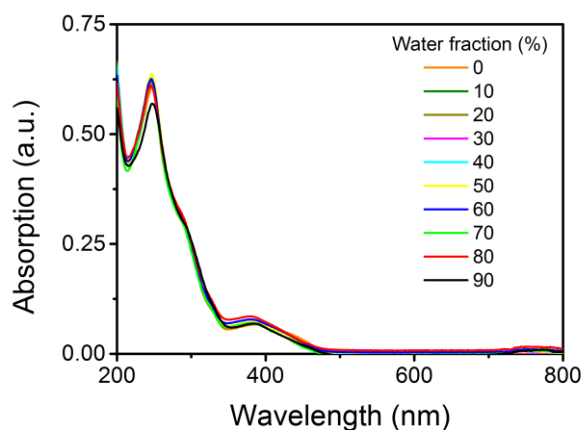


Fig. S4 The absorption spectra of complex **1** in water-CH₃CN mixtures with different water fractions (0–90% v/v) at room temperature.

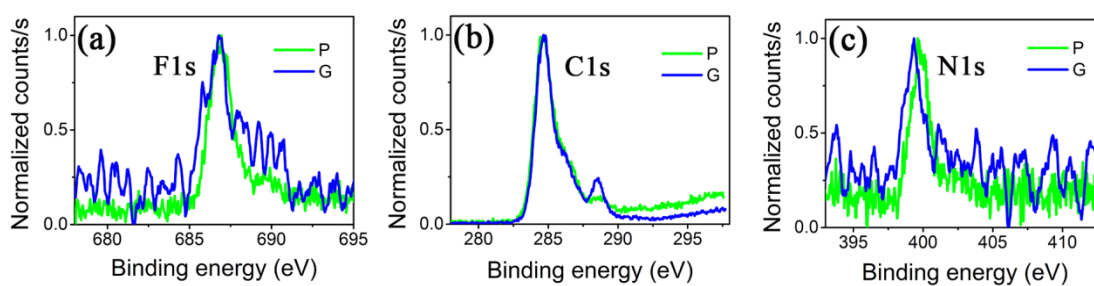


Fig. S5 XPS spectra of F 1s, C 1s and N 1s for complex **1**